

# Abnormal Reverse Intersystem Crossing of Polaron-Pair States and Its Conversion to Intersystem Crossing via the Regulation of Intermolecular Electron-Hole Spacing Distance

Jing Xu,<sup>1</sup> Xiantong Tang,<sup>1</sup> Xi Zhao,<sup>1</sup> Hongqiang Zhu<sup>2,†</sup>, Fenlan Qu,<sup>1</sup> and Zuhong Xiong<sup>1,\*</sup>

<sup>1</sup>*School of Physical Science and Technology, MOE Key Laboratory on Luminescence and Real-Time Analysis, Southwest University, Chongqing 400715, People's Republic of China*

<sup>2</sup>*Chongqing Key Laboratory of Photo-Electric Functional Materials, Chongqing Normal University, Chongqing 401331, People's Republic of China*

(Received 12 November 2019; revised 21 May 2020; accepted 26 June 2020; published 6 August 2020)

Reverse intersystem crossing (RISC) unexpectedly dominates the interconversion of polaron pairs in the traditional fluorescent material 4-(dicyanomethylene)-2-*tert*-butyl-6-(1,1,7,7-tetramethyljulolidin-4-yl-vinyl)-4*H*-pyran (DCJTB), with a large energy gap ( $\Delta E_{ST}$ ) between singlet and triplet excitons, by employing the magnetoelectroluminescence detection technique. Contrary to RISC among excitons with small  $\Delta E_{ST}$  from conventional thermally activated delayed fluorescence, these RISC processes are increased at a high current density and low temperature, which is ascribed to an enhanced direct charge-trapping effect and prolonged lifetime of the triplet-polaron pair, respectively. More intriguingly, the conversion of RISC to ISC is observed by reducing the electron-hole distance of polaron pairs via increasing the concentration of DCJTB dopant. Furthermore, the host must have a high triplet exciton energy to prevent energy back-transfer of the triplet exciton from the guest to the host and ensure efficient occurrence of the RISC process. The RISC-dominated device has a markedly higher external quantum efficiency than that of the ISC-governed one. This work not only deepens the microscopic understanding of the spin-pair states of red-light-emitting DCJTB-doped devices, but also provides a useful method to utilize a conventional fluorescent dopant for designing high-efficiency organic light-emitting diodes.

DOI: 10.1103/PhysRevApplied.14.024011

## I. INTRODUCTION

Organic light-emitting diodes (OLEDs) possessing high luminous efficiency have always been an important topic in the organic optoelectronic field. In most traditional fluorescent OLEDs, the external quantum efficiency (EQE) is limited to 5% [1,2], which is problematic for meeting industrial demands. To overcome this limitation, Kim *et al.* [3–6] reported a series of high-efficiency phosphorescent OLEDs containing noble or rare metals via utilization of their spin-orbit coupling interactions. However, phosphorescent OLEDs suffer from high material costs and face a lack of resources in the future. Further, Adachi *et al.* [7–9] have achieved a high EQE by designing and synthesizing intermolecular and intramolecular charge-transfer (CT) materials, i.e., exciplex and thermally activated delayed fluorescence (TADF) materials; this high EQE is the result of reverse intersystem crossing (RISC) from CT<sup>3</sup> to CT<sup>1</sup> and then their radiative recombination. For RISC to occur efficiently, a small energy gap ( $\Delta E_{ST}$ )

between CT<sup>3</sup> and CT<sup>1</sup> is required, which can realize the upconversion of CT<sup>3</sup> to CT<sup>1</sup>. However, these CT materials require complicated and troublesome chemical syntheses, which results in their limited application [7]. Thus, an alternative approach focuses on obtaining a better performance of OLEDs on the basis of resource saving and fabrication convenience, for example, through an in-depth mechanistic study of some traditional fluorescent materials. In addition, compared with most TADF materials, conventional fluorescent materials are more stable, which makes them have an inherently long device lifetime.

As is reported in the literature, 4-(dicyanomethylene)-2-*tert*-butyl-6-(1,1,7,7-tetramethyljulolidin-4-yl-vinyl)-4*H*-pyran (DCJTB) is widely used as a red-fluorescent dopant for high-efficiency OLEDs. Zhao *et al.* provided a strategy to achieve the red-light emission of DCJTB with an EQE of 10.15% by doping 1% DCJTB into the cohosts of 4,4',4''-tri(9-carbazoyl)triphenylamine (TCTA) and 2,4,6-tris[3-(1*H*-pyrazol-1-yl)phenyl]-1,3,5-triazine (3P-T2T) [10]. In addition, Zhou *et al.* used (*E*)-9-{4-[2-(anthracen-9-yl)vinyl]phenyl}-10-(naphthalen-1-yl)anthracene (APEAn1N)/tris-(8-hydroxyquinolinato)aluminum Alq<sub>3</sub>:DCJTB to obtain a stable white-light OLED [11]. However,

\*zhxiong@swu.edu.cn

†20132013@cqnu.edu.cn

there are few reports that give a detailed understanding of the basic luminescence mechanism and the evolution of excited states in DCJTB-doped OLEDs. Recently, the magnetoelectroluminescence (MEL) from OLEDs has been widely utilized as an effective detection technique to investigate the fundamental luminescence mechanisms that occur within OLEDs [12–14]. This is because these MEL traces can exhibit sensitive fingerprint responses to complex spin interactions among electron-hole (*e-h*) pairs, such as ISC [13,15], RISC [16,17], and triplet-triplet annihilation (TTA) [18,19]. Based on this sensitive MEL tool, Chen *et al.* discovered RISC and TTA from the emitting layer of 4% DCJTB-doped 1,3-bis(*N*-carbazolyl)benzene (mCP) and proposed that RISC and TTA were both produced from excitons of DCJTB [20]. Since the MEL curves are analyzed only at a fixed DCJTB concentration of 4%, it is difficult to fully disclose and reasonably explain the microscopic mechanisms of spin-related processes occurring in DCJTB-doped OLEDs.

Here, we select the exciplex of TCTA:2,4,6-tris[3-(diphenylphosphinyl)phenyl]-1,3,5-triazine (PO-T2T) as the host and DCJTB as the guest to fabricate conventional high-efficiency fluorescent DCJTB-doped OLEDs and systematically investigate the dependences of MEL curves on device current density, working temperature, and doping concentration. Surprisingly, it is found that an abnormal RISC process, which is enhanced at a high current density and low operational temperature, occurs among DCJTB polaron pairs, rather than DCJTB excitons, and this RISC could unexpectedly convert to ISC of DCJTB polaron pairs when the electron-hole distance of polaron pairs in the DCJTB dopant molecules is reduced via increasing its doping concentration. Moreover, the occurrences of spin-pair microscopic processes containing RISC, ISC, and TTA

significantly depend on the device operational conditions. Specifically, if the DCJTB concentration is low, RISC governs the interconversion between singlet- and triplet-polaron pairs in DCJTB, otherwise ISC is dominant. Moreover, the RISC-dominated device has a markedly higher EQE than that of the ISC-governed one. Additionally, at a high current density and low temperature, the MEL curves are attributed to RISC of DCJTB polaron pairs and TTA of DCJTB excitons, whereas, at a low current density and high temperature, ISC of the exciplex and TTA of DCJTB excitons dominate. This complicated behavior of excited states in DCJTB-doped exciplex OLEDs can be interpreted by employing exciton energy transfer (ET) and direct charge trapping (DCT). Our research is of great value for providing a deeper understanding of spin-pair state micromechanisms for RISC and TTA coexisting in light-emission systems and for revealing how to obtain a high luminous efficiency using a conventional fluorescent dopant material.

## II. EXPERIMENTAL SECTION

All devices studied here are fabricated by organic molecular beam deposition under high vacuum ( $\sim 10^{-6}$  Pa). The structure of our core device (Dev. 1) is indium tin oxide (ITO)/poly(3,4-ethylenedioxythiophene):poly(styrene-sulfonate) (PEDOT:PSS) (30 nm)/4,4',4''-tris(*N*-3-methylphenyl-*N*-phenylamino)triphenylamine (*m*-MTDATA) (40 nm)/TCTA(20 nm)/TCTA:PO-T2T:5%DCJTB(40 nm)/PO-T2T(50 nm)/LiF(1 nm)/Al(120 nm), where PEDOT:PSS, *m*-MTDATA, TCTA, TCTA:PO-T2T:5%DCJTB, and PO-T2T are used as the hole-injection layer, hole-transporting layer, exciton-blocking layer, emission layer (EML), and electron-transporting layer, respectively.

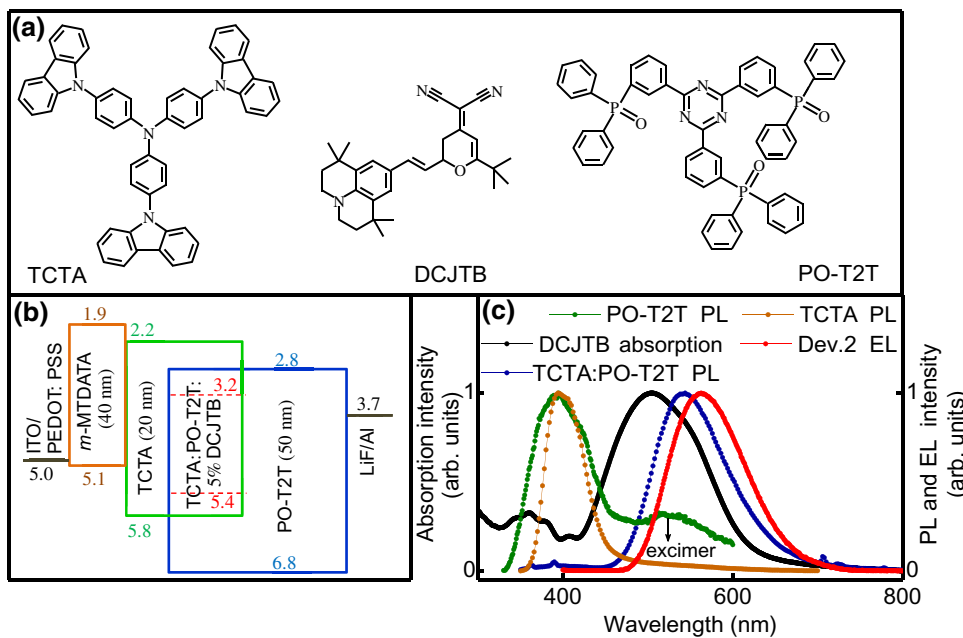


FIG. 1. (a) Molecular structures of TCTA, DCJTB, and PO-T2T. (b) Energy-level structure of Dev. 1. (c) Normalized PL spectra of TCTA, PO-T2T, and TCTA:PO-T2T films; EL spectra of Dev. 2; and absorption spectrum of DCJTB film.

Meanwhile, to better analyze spin interactions among  $e-h$  pairs in Dev. 1 and considering that TCTA and PO-T2T are prone to forming exciplexes, we target the EML of Dev. 1 [the molecular structure of the materials used are shown in Fig. 1(a)] to prepare Dev. 2, Dev. 3, and Dev. 4 as control devices, the EMLs of which are TCTA:PO-T2T, TCTA:5% DCJTB, and Alq<sub>3</sub>:5% DCJTB, respectively, while maintaining other functional layers and their thicknesses, as well as the EML thickness, unchanged. Furthermore, the optical, electrical, and magnetic properties, including the MEL traces, EQE, photoluminescence (PL), electroluminescence (EL), and absorption spectra; current density-voltage-brightness; and temperature dependences of these devices are measured with the following experimental instruments: electromagnet EM 4 (powered by Lakeshore: EM647), Gaussmeter (Lakeshore 421), Keithley 2400 source meter, Keithley 2000 multimeter, brightness meter (ST-86LA), SpectraPro-2300i grating spectrometer, ultraviolet and visible spectrophotometer (UV-2600), SpectraScan PR705, and a closed-cycle cryostat (Janis CCS-350S).

### III. RESULTS AND DISCUSSION

#### A. Energy level structure and optical and electric properties

Figure 1(b) shows the energy-level structure of Dev. 1. It can be seen that the energy differences of the highest occupied molecular orbital (HOMO) between TCTA and PO-T2T and the lowest unoccupied molecular orbital (LUMO) between TCTA and PO-T2T are 1.0 and 0.6 eV, respectively. These large energy-level differences will result in pronounced accumulation of electrons and holes at the interface of TCTA/PO-T2T, to generate strong exciplex emission due to the electron transition from the LUMO of PO-T2T to the HOMO of TCTA. This transition process can be confirmed by comparing the PL spectra of films of the materials TCTA, PO-T2T, and TCTA:PO-T2T presented in Fig. 1(c). Clearly, the PL of the exciplex (TCTA:PO-T2T) shows a notable redshift to 554 nm, with respect to the TCTA exciton emission located at 394 nm and the PO-T2T exciton emission at 395 nm. As for the featureless broad emission of PO-T2T with a maximum at 520 nm, it is assigned to excimer emission of the PO-T2T film [21,22]. Due to the mutual interactions between molecules, generation of the excimer will reduce the energy of the excited states, so that the PL spectrum of the excimer will display a redshift compared with the PL spectrum of its singlet excitons.

After doping DCJTB into the exciplex host, it is found that the HOMO and LUMO levels of DCJTB are completely surrounded by those of the exciplex [Fig. 1(b)], and the HOMO energy-level offset between TCTA and DCJTB and the LUMO energy-level offset between PO-T2T and DCJTB are both 0.4 eV, indicating that DCJTB molecules

may act as trap sites for both holes and selectrons. Thus, there is a DCJTB emission partially from the direct radiative recombination of trapped electrons and holes, i.e., some DCT processes of charge carriers exist in Dev. 1. Moreover, as observed in Fig. 1(c), the PL spectrum of the exciplex overlaps well with the absorption spectrum of DCJTB, indicating that efficient ET can also occur from the exciplex to DCJTB molecule. That is, DCJTB molecules can obtain exciton energy by Förster resonance energy transfer (FRET) or Dexter energy-transfer (DET) processes. FRET occurs at a low doping concentration among singlet excited states because it is a long-range resonant energy transfer through a dipole electrostatic coupling. Moreover, DET occurs at high doping concentrations among excited states because it is a short-range interaction and requires an electron-exchange process [23–26]. Recently, Kirch *et al.* reported that FRET could also occur from the triplet excited state of the donor to the singlet excited state of the acceptor by using a bioluminescent *N,N'*-di(naphthalene-1-yl)-*N,N'*-diphenylbenzidine (NPB) host doped with a red-fluorescent DCJTB guest [27]. Notably, this bioluminescent NPB host material has two emission peaks in the PL spectrum at room temperature, which are, respectively, emitted from triplet and singlet excited states. Moreover, RISC in NPB molecules is not taken into account because of the large singlet-triplet energy difference,  $\Delta E_{ST} \approx 0.55$  eV, of the NPB donor. Thus, in addition to the normal FRET of the singlet exciton from the host to the guest, FRET from the triplet exciton of the NPB host to the singlet exciton of the DCJTB guest may occur. Nevertheless, in our work, the exciplex (TCTA:PO-T2T) is used as a host and has no property of bioluminescent emission. This is because there is only one peak in the PL spectrum from this exciplex at room temperature [Fig. 1(c)], indicating the sole emission of singlet exciplex states. In addition, this exciplex has a negligible single-triplet energy difference ( $\Delta E_{ST} \approx 0$  eV), leading to the efficient occurrence of the RISC process. Therefore, there are almost no net triplet excitons in the host exciplex and the FRET process from the triplet exciton of the donor (TCTA:PO-T2T) to the singlet exciton of the acceptor (DCJTB) can be ignored in this study. Based on the above analyses, we believe that DCT and ET processes (including FRET and DET, depending on the specific contents of DCJTB dopant) exist in Dev. 1. Obviously, they together regulate the mutual transformation of these spin-pair states in the exciplex host and DCJTB guest molecules, and thus, affect the optical, electric, and magnetic properties of our studied devices, as demonstrated below in detail.

#### B. Current-density- and temperature-dependent MEL traces of Dev. 1 and Dev. 2

Figures 2(a) and 2(b) show the current-density dependence of MEL curves obtained at different magnetic

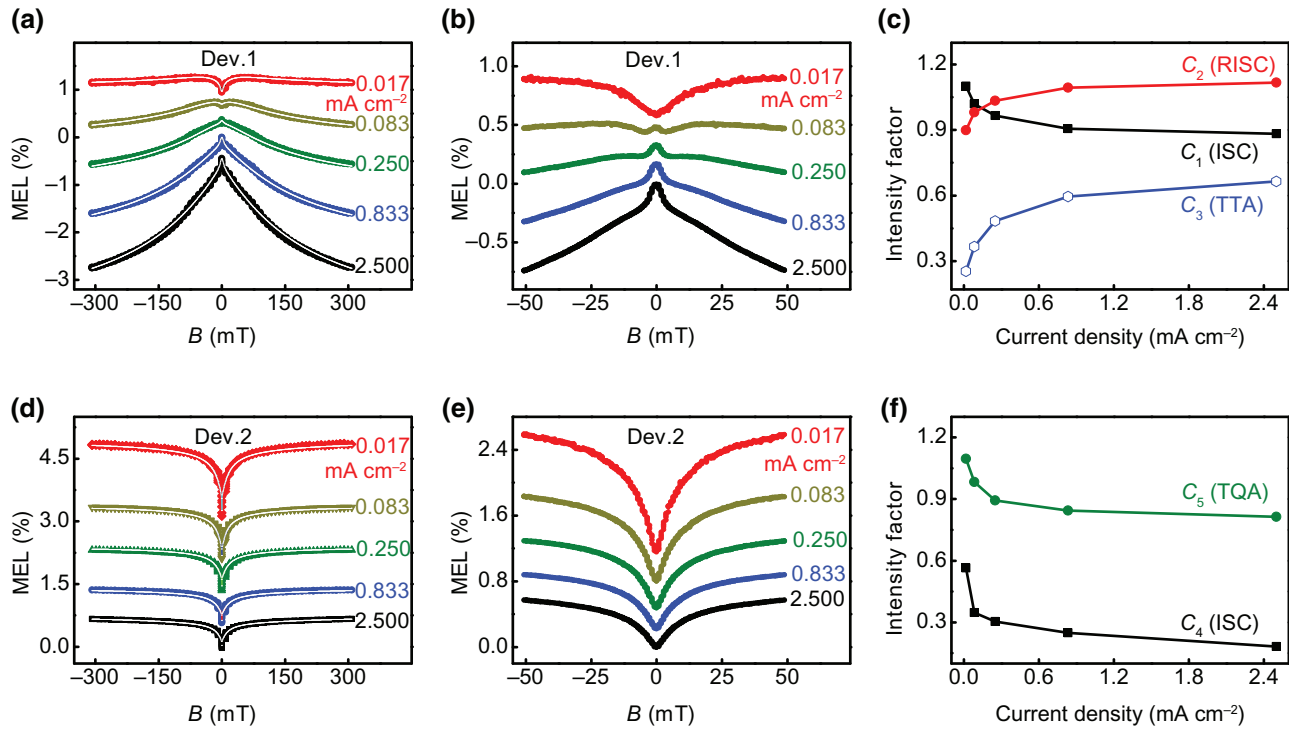


FIG. 2. (a),(b) Current-density-dependent MEL curves of Dev. 1 at 300 K within the field ranges of  $|B| < 300$  and 50 mT, respectively. MEL curves are offset for clear observation. White solid lines in (a) are fitted curves from Dev. 1. (c) Current-density dependences of the intensity factors ( $C_1$ ,  $C_2$ , and  $C_3$ ) used for describing the occurrence magnitude of ISC, RISC, and TTA, respectively. (d),(e) MEL curves of Dev. 2 at 300 K within the field ranges of  $|B| < 300$  and 50 mT. MEL curves are offset for clear observation. White solid lines in (d) are fitted curves from Dev. 2. (f) Current-density dependences of the intensity factors ( $C_4$  and  $C_5$ ) used for describing the occurrence magnitude of ISC and TQA, respectively.

field ( $B$ ) ranges of 300 and 50 mT from Dev. 1 using an exciplex of TCTA:PO-T2T doped with 5% DCJTb as an emission layer. The MEL is defined as  $MEL = (\Delta EL)/(EL) = [EL(B) - EL(0)] \times 100\% / EL(0)$ , where  $EL(B)$  and  $EL(0)$  are the EL intensities in the presence and absence of an external  $B$ , respectively. The typical MEL line shapes of  $B$ -mediated ISC, RISC, and TTA processes are shown in Fig. S1 within the Supplemental Material [28], and their physical origins are interpreted in detail in the first part of Supplemental Material [28–33]. As depicted in Figs. 2(a) and 2(b), all of these MEL curves of Dev. 1 are composed of low-field and high-field components. The low-field effects present a rather sharp increase or decrease around zero field, depending on the magnitude of current density. As reported in the literature [13,14,31], they are the fingerprint curves originating from  $B$ -mediated ISC and RISC processes between singlet- and triplet-polaron pairs or charge-transfer excitons, which have inverted-Lorentzian- and Lorentzian-type traces, respectively. Moreover, if the OLED has only one pure emission layer (e.g., the conventional device of ITO/NPB/Alq<sub>3</sub>/LiF/Al), its magnetic response curve solely originates from the single microscopic mechanism (i.e.,  $B$ -mediated ISC process of Alq<sub>3</sub> polaron pairs)

[34,35]. However, if the emission layer of an OLED is a doped film, such as the host-guest and even host-sensitizer-guest systems, its MEL curve should be determined by the overlapping effect of the magnetic field responses from these functional materials, depending on the exciton energy-transfer processes occurring in the emission layer [29,36]. Therefore, the low-field positive to negative conversion in Figs. 2(a) and 2(b) can be understood as competition of the ISC of the exciplex with RISC of DCJTb. The high-field components exhibit a gradual saturation or decrease, depending on the strength of TTA [18,37]. In other words, ISC, RISC, and TTA are the main physical mechanisms in Dev. 1, and they work together to form different kinds of MEL traces for Dev. 1. To explore the formation mechanism of excitons in Dev. 1, we measure the MEL curves of Dev. 2 using only an exciplex of TCTA:PO-T2T as an emission layer, as shown in Figs. 2(d) and 2(e) for  $B$  ranges of 300 and 50 mT, respectively. The MEL curves increase sharply and gradually within small and large  $B$ , which can be attributed to the ISC- and triplet-charge annihilation (TQA) induced MEL traces, respectively [38–40]. As for the reactions between the triplet exciton and charge or polaron in an OLED, triplet-polaron quenching (TPQ) [41,42] or triplet-polaron

interaction (TPI) [43,44] are also commonly used terms. An explanation of the small differences in this nomenclature can be found in the Supplemental Material [14,28,41–50]. Therefore, based on the MEL comparison of Figs. 2(a) and 2(b) with Figs. 2(d) and 2(e), we can conclude that the RISC and TTA in Dev. 1 (TCTA:PO-T2T:5%DCJTB) are produced only from DCJTB molecules.

As reported in the literature, DCJTB is a traditional red-fluorescent material with a large singlet-to-triplet exciton energy gap of  $\Delta E_{ST}$  (0.352 eV), compared with CT materials (usually with  $\Delta E_{ST} < 0.1$  eV) [7,20]. This means that the RISC process does not occur among excitons of DCJTB. Thus, the RISC of Dev. 1 occurs only from the polaron pairs of DCJTB, and TTA occurs among DCJTB excitons. Here, we introduce the rate constants for exciton generation from singlet- and triplet-polaron-pair states, which are denoted  $k_S$  and  $k_T$ , respectively. It is reported [15,29,30] that, if the EL intensity of OLEDs decreases sharply in the presence of a small  $B$  (i.e., RISC-induced MELs),  $k_S$  is larger than that of  $k_T$ . On the contrary,  $k_S$  is smaller than that of  $k_T$  if the EL intensity increases rapidly in the presence of  $B$  (i.e., ISC-induced MELs). The full width at half maximum of RISC-induced or ISC-induced MELs is in the order of a few millitesla [31,51,52], which is mainly reflected by the low-field MEL curves. Thus, it is reasonably believed that the formation rate of DCJTB excitons satisfies the condition of  $k_S > k_T$  in Dev. 1, which can be further confirmed by the MEL curves obtained at a high current density [Fig. 2(b)]. It is reported that the line shape of TTA-induced MEL is characteristic, with a small increase at small  $B$  and then a slow decrease at large  $B$  after reaching a maximum at around 20 mT [30]. Although this line shape is irrespective of the relative values of  $k_S$  and  $k_T$ , the occurrence strength of TTA can be modulated by the relative values of  $k_S$  and  $k_T$  through changing the quantity of the triplet exciton, which is mainly reflected in the high-field MEL curves. To discuss these processes quantitatively, we utilize the combination of Lorentzian and non-Lorentzian functions to fit the complex experimental MEL curves [53,54]. The MEL curves displayed in Figs. 2(a) and 2(d) can be fitted by

$$\text{MEL} = C_1 \frac{B^2}{B^2 + B_1^2} - C_2 \frac{B^2}{B^2 + B_2^2} + C_3 \left[ A_1 \frac{B^2}{B^2 + B_3^2} - A_2 \frac{B^2}{(|B| + B_4)^2} \right], \quad (1)$$

$$\text{MEL} = C_4 \frac{B^2}{B^2 + B_5^2} + C_5 \frac{B^2}{(|B| + B_6)^2}. \quad (2)$$

In Eq. (1), the first term models ISC, while the second and third terms represent RISC and TTA processes, respectively.  $C_1$ ,  $C_2$ , and  $C_3$  are the intensity factors that

represent these three reaction channels occurring under different experimental conditions. In Eq. (2), the first term models ISC, but the second one is for the TQA process.  $C_4$  and  $C_5$  are the intensity factors that represent these two reaction channels occurring under different experimental conditions. It can be seen from Figs. 2(a) and 2(d) that these fitted traces (white solid lines) are consistent with the experimentally obtained curves. As shown in Figs. 2(c) and 2(f), when the current density increases, ISC in Dev. 1 is weakened and TTA is enhanced, while ISC and TQA in Dev. 2 are weakened; these observations are in good agreement with reports in the literature [18,31,36,55]. Additionally, the RISC process of Dev. 1 is abnormally increased, which is interpreted in detail below.

Considering that the operational temperature of our DCJTB-doped device usually affects its carrier mobility and the formation probability of spin-pair states [14, 36], the temperature-dependent MEL curves of Dev. 1 are measured within  $B$  ranges of 300 and 50 mT, as shown in Figs. 3(a) and 3(b), respectively. As observed, although these MEL curves still exhibit TTA behavior of DCJTB excitons, as exhibited by a high-field component [Fig. 3(a)]; the RISC process of DCJTB polaron-pair (PP) states; and the ISC process of the exciplex by low-field components [Fig. 3(b)], the occurrence of these three mechanisms changed dramatically with decreasing temperature. To intuitively understand these changes, we also use Eq. (1) to fit the MEL curves depicted in Fig. 3(a) and obtain the corresponding fitted curves. Clearly, the fitted traces are in good agreement with the experimentally tested curves. Moreover, the relationship between intensity factor  $C_1$  and temperature in Fig. 3(c) demonstrates that ISC weakens as the temperature decreases, which is similar to reports in the literature [14,56]. Surprisingly, the intensity factors  $C_2$  and  $C_3$  show that RISC is enhanced and TTA is weakened with decreasing temperature, both of which are contrary to related reports in the literature [13,36].

For TTA and RISC processes occurring in OLEDs, they have their own variation rules with the working temperature of device. Usually, the TTA process is enhanced with decreasing temperature because the disturbance of thermal phonons is reduced, leading to a prolonged lifetime of triplet excitons and improved TTA at low temperatures [13]. The rate constant ( $k_{RISC}$ ) for the RISC process satisfies the following equation:  $k_{RISC} = A \exp(-\Delta E_{ST}/k_B T)$ , where  $A$  is a constant,  $\Delta E_{ST}$  is the singlet-triplet energy gap,  $k_B$  is the Boltzmann constant, and  $T$  is the temperature. Thus, the RISC process should be weakened with decreasing temperature [17]. In fact, these theoretical analyses are contrary to our experimental results, as displayed by the intensity factors  $C_2$  and  $C_3$ .

### C. Microscopic mechanistic analysis of Dev. 1

Combining the current-density- and temperature-dependent MEL curves of Dev. 1 shown in Figs. 2 and 3 with

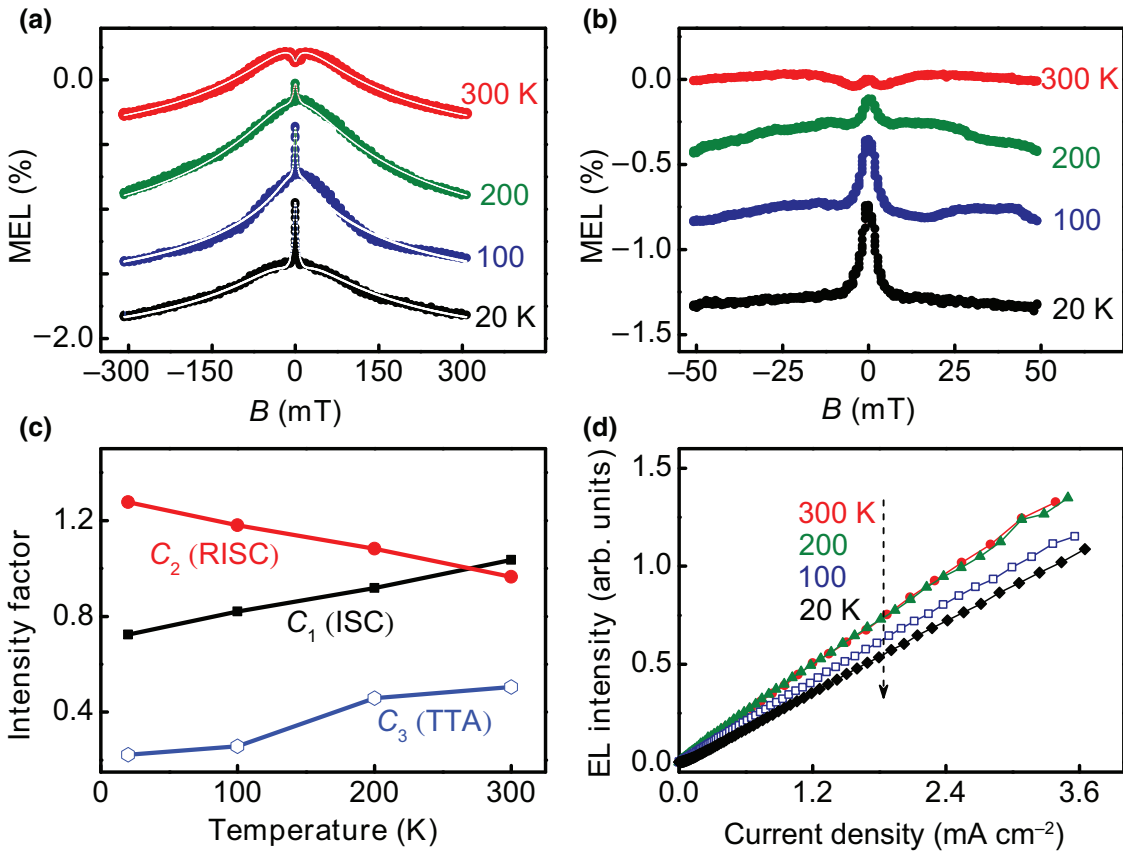


FIG. 3. (a),(b) Temperature-dependent MEL curves of Dev. 1 acquired at  $0.083 \text{ mA/cm}^2$  within the field ranges of  $|B| < 300$  and  $50 \text{ mT}$ , respectively. MEL curves are offset for clear observation. White solid lines in (a) are the fitted curves from Dev. 1. (c) Relationship between the intensity factors ( $C_1$ ,  $C_2$ , and  $C_3$ ) and temperature. (d) Brightness-current-density characteristics of Dev. 1 at different temperatures.

well-known device physics for the host-guest system of OLEDs, we propose a diagram illustrating the microscopic mechanism occurring in the emission layer, consisting of the exciplex host of TCTA:PO-T2T doped with the DCJTB guest at low concentrations, as displayed in Fig. 4.

As shown in Fig. 4, under electric excitation, a portion of electrons and holes injected from the cathode and anode recombine in the emission layer to form singlet- and triplet-polaron pairs ( $\text{PP}^1$  and  $\text{PP}^3$ ) in the exciplex molecules of TCTA:PO-T2T. Subsequently,  $\text{PP}^1$  and  $\text{PP}^3$  form the corresponding singlet and triplet exciplex excitons ( $\text{EX}_1$  and  $\text{EX}_3$ ). Moreover, both PP and EX states have their own MEL curves [13,15,57]. Due to the negligible spin-exchange energy of the PP states, both ISC ( $\text{PP}^1 \rightarrow \text{PP}^3$ ) and RISC ( $\text{PP}^1 \leftarrow \text{PP}^3$ ) processes simultaneously occur and compete with each other, but the major process is determined by the dominant fingerprint MEL traces. For the EX states ( $\text{EX}_1$ ,  $\text{EX}_3$ ), the ISC process ( $\text{EX}_1 \rightarrow \text{EX}_3$ ) is ignored because the lifetime of  $\text{EX}_1$  is very short, due to its fast evolution for producing the singlet DCJTB excitons through the FRET channels. That is, only the RISC process ( $\text{EX}_1 \leftarrow \text{EX}_3$ ) is considered,

due to the long lifetime of  $\text{EX}_3$  and the relatively small spin-exchange energies of the EX states. As shown in Fig. 2(d), the comprehensive MEL traces induced from the  $B$ -modulated evolution channels of PP and EX states in the exciplex host reveal that the net ISC process is the major one. This means that the ISC process ( $\text{PP}^1 \rightarrow \text{PP}^3$ ) is stronger than the RISC one ( $\text{PP}^1 \leftarrow \text{PP}^3$ ) in PP states and stronger than the RISC process ( $\text{EX}_1 \leftarrow \text{EX}_3$ ) of the EX states because ISC and RISC processes have opposite MEL curves, and MEL is an overlapping effect. Thus, the evolution channels of the PP and EX states in the exciplex host of TCTA:PO-T2T should be expressed as  $\text{PP}^1 \rightleftharpoons \text{PP}^3$  and  $\text{EX}_1 \leftarrow \text{EX}_3$ , respectively, as displayed in the top panel of Fig. 4.

For the DCJTB guest at low doping concentrations, the excited states formed in the DCJTB guest come from the following two pathways. One is produced from the exciplex host via the FRET process, consequently generating some singlet DCJTB excitons ( $S_1$ ). Apparently, this pathway will generate the MEL response (reflecting the ISC process) originating from  $B$ -mediated PP states of the exciplex host. The other is the formation of PP states ( $\text{PP}^1$

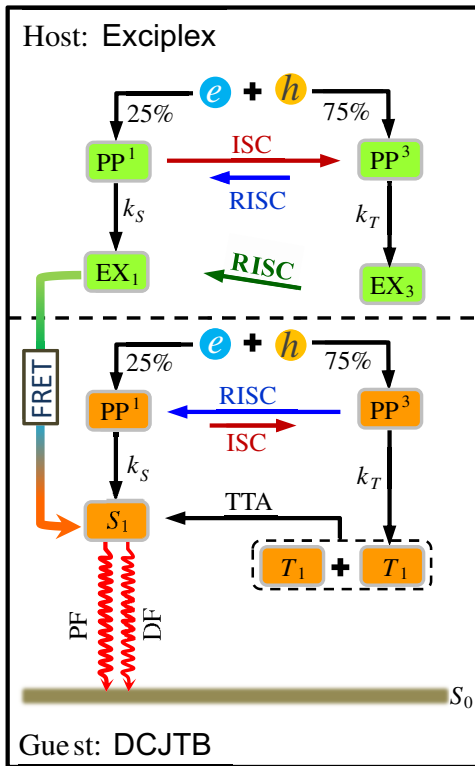


FIG. 4. Micromechanistic diagrams of Dev. 1 operating at a low DCJTB doping concentration.

and  $\text{PP}^3$ ) through the DCT process, and then these PP states rapidly evolve into the singlet and triplet excitons ( $S_1$  and  $T_1$ ) of DCJTB. Moreover, at low DCJTB concentration,  $\text{PP}^1$  and  $\text{PP}^3$  states are degenerate in energy levels, so both ISC ( $\text{PP}^1 \rightarrow \text{PP}^3$ ) and RISC ( $\text{PP}^1 \leftarrow \text{PP}^3$ ) processes of these PP states simultaneously occur and compete with each other, but the major process can be determined through analyzing the dominant MEL curves. Clearly, independent of the DCJTB content,  $S_1$  is higher in energy by over 0.352 eV than that of  $T_1$ , which means that RISC ( $S_1 \leftarrow T_1$ ) is absent, because the energy barrier of 0.352 eV is too large for  $T_1$  to overcome. In addition, the ISC ( $S_1 \rightarrow T_1$ ) is ignored, due to the short lifetime of  $S_1$  because of its fast evolution for producing fluorescence through an irradiative decay. Therefore, for the DCJTB guest at low doping concentrations, we can consider only the evolution channels (ISC and RISC) of the PP states, and the major channel can be determined by comparing the low-field MEL traces of Dev. 1 and Dev. 2. As observed in Fig. 2(a), the low-field MEL traces of Dev. 1 (TCTA:PO-T2T:5%DCJTB) show weak ISC and RISC processes at low and high current density, respectively; however, Dev. 2 (TCTA:PO-T2T) solely displays strong ISC processes for all current density in Fig. 2(d). Thus, the RISC process in Fig. 2(a) must result from the evolution channel  $\text{PP}^1 \rightleftharpoons \text{PP}^3$  of the PP states in DCJTB guest molecules, because ISC and RISC processes have

opposite MEL curves and MEL is an overlapping effect. In addition, the high-field MEL traces of the Dev. 1 show that TTA ( $T_1 + T_1 \rightarrow S_1 + S_0$ ) processes are present, especially at a high current density. Therefore, the evolution channels of the PP states and the triplet exciton states in the DCJTB guest should be expressed as  $\text{PP}^1 \rightleftharpoons \text{PP}^3$  and  $T_1 + T_1 \rightarrow S_1 + S_0$ , which are displayed in the bottom panel of Fig. 4.

When the current density is small, a part of the injected charge carriers is located on the TCTA:PO-T2T host molecules, and another part of the injected charge carriers is directly trapped by the DCJTB guest molecules. The carriers on the host molecules will produce PP states and exciplex excitons (EX<sub>1</sub> and EX<sub>3</sub>), and the ones on the guest molecules will form DCJTB PP states and excitons (S<sub>1</sub> and T<sub>1</sub>). As shown in Figs. 2(a) and 2(d), the low-field MEL magnitudes of Dev. 1 are very small, relative to those of Dev. 2. So, it is reasonably concluded that the quantity of the resultant PP states is a little larger in the exciplex molecules of TCTA:PO-T2T than those in the DCJTB guest molecules at low current densities (<0.083 mA/cm<sup>2</sup>), because ISC and RISC processes have opposite MEL traces and MEL is an overlapping effect. Thus, the MEL curves exhibit ISC-dominated feature. As the current density increases, the FRET effect from EX<sub>1</sub> to S<sub>1</sub> gradually saturates [58]. At the same time, DCJTB will capture a large number of electrons and holes and produce many PP states, resulting in the dominant RISC process of DCJTB polaron pairs.

Additionally, as the current density increases, the number of triplet excitons of DCJTB will exponentially rise, leading to enhanced TTA because TTA is proportional to the square of the number of triplet excitons [31,37]. Hence, the current-density-dependent MEL curves shown in Figs. 2(a) and 2(b) are obtained. As the temperature decreases, there is an increase in the RISC process because the lifetime and number of PP<sup>3</sup> in DCJTB increase. Additionally, enhanced RISC can result in a decrease in the number of triplet excitons, leading to weakened TTA, as shown by the intensity factor C<sub>3</sub> in Fig. 3(c). Since PP states are important intermediate states, which can further form excitons or dissociate into free charges [14,59], only part of PP<sup>1</sup> generated by the RISC process takes part in forming S<sub>1</sub> of DCJTB to produce prompt fluorescence. Meanwhile, weakened TTA can reduce delayed fluorescence. Clearly, the comprehensive contributions of these three mechanisms of ISC, RISC, and TTA occurring in Dev. 1 cause the decreased EL intensity of Dev. 1 as the temperature decreases, as shown in Fig. 3(d).

#### D. Concentration-dependent MEL traces of DCJTB-doped devices

To fully understand the microscopic mechanisms reflected by MEL traces in DCJTB-doped devices, it is

necessary for us to detect the room-temperature MEL curves attained at different DCJTB concentrations. It is well known that molecular aggregation effects [60] will be more pronounced with an increase of DCJTB concentration, which is prone to the occurrence of exciton quenching [60,61]. Thus, we adopt DCJTB doping concentrations up to a maximum of 16%. The EL spectra of DCJTB-doped devices will generate redshifts with increasing DCJTB concentration [Fig. 5(a)], which proves the above point of view [61]. The MEL curves of these devices with various DCJTB doping concentrations are shown in Fig. 5(b). Obviously, the high-field MEL traces look similar at different DCJTB concentrations (i.e., each MEL trace exhibits a slow decrease with increasing  $B$ ), which is always a feature of TTA behavior. Surprisingly, a sharp rise (i.e., ISC process) in the low-field MEL curves is observed at high DCJTB concentrations (16%, 10%, and 8%), which is sharply in contrast to the rapid decrease (i.e., RISC process) at low DCJTB concentrations (5% and 2%). As concluded above, the RISC process occurring in DCJTB molecules is derived from their PP states via comparing and analyzing the MEL line shapes of Dev. 1 and Dev. 2. These PP states are important intermediate states, because the observed EL is produced from the recombination of a large number of singlet excitons evolved from their precursors of PP states. Moreover, the spin flips of these PP states can be modulated under a small  $B$ , i.e., occurring ISC ( $\text{PP}^1 \rightarrow \text{PP}^3$ ) or RISC ( $\text{PP}^3 \rightarrow \text{PP}^1$ ) processes. Normally, electrons and holes of polaron pairs are well separated and their exchange splitting energies are negligible, so  $\text{PP}^1$  and  $\text{PP}^3$  states are degenerate. In this case, ISC or RISC processes may occur, depending on the relative values of  $k_S$  and  $k_T$ . Deng *et.al* [36] conducted a detailed study on the dependence of the low-field MEL curves on the guest concentration for the host-guest doping system, which indicated that a larger guest concentration resulted in a more obvious microscopic process occurring in the guest material. According to this conclusion, we should obtain more negative low-field MEL curves by increasing the concentration of DCJTB, but, factually, positive low-field MEL curves are obtained in our DCJTB-doped devices, as shown in Fig. 5(b). In addition, the low-field MEL curves are more positive upon further increasing the DCJTB concentration. Clearly, this is sharply in contrast to the typical characteristics of the RISC process (i.e., a conventional TADF feature). Thus, we infer that there must be other dynamic changes occurring in DCJTB molecules when the concentration of DCJTB increases.

Under electric excitation, the electrons and holes injected from individual electrodes move toward the emission layer of the device, leading to the formation of  $e-h$  pairs in the emission layer due to their mutual Coulomb attraction. It is known that the positions of the electron and hole in  $e-h$  pairs are dynamic and will change over time. This makes the interactions among polaron pairs

more complicated because the variation of the electron-hole separation distance can cause fluctuations in the value of the exchange coupling. The exchange coupling energy,  $J$ , satisfies [62]

$$J = \iint \varphi_n^*(\mathbf{r}_1)\varphi_k(\mathbf{r}_1) \frac{1}{|\mathbf{r}_1 - \mathbf{r}_2|} \varphi_n(\mathbf{r}_2)\varphi_k^*(\mathbf{r}_2) d^3\mathbf{r}_1 d^3\mathbf{r}_2,$$

with  $\varphi_n$  and  $\varphi_k$  corresponding to the electron and hole orbitals, respectively. Often  $\varphi_n$  is the LUMO and  $\varphi_k$  is the HOMO. If the electron and hole orbitals are localized and spatially separated,  $J$  decays rapidly (typically exponentially) with the electron-hole separation [63,64]. Even a subtle change in the PP-state configuration can result in significant variations in the energy gap between  $\text{PP}^1$  and  $\text{PP}^3$  states. Lee *et al.* [64] proposed a microscopic dynamics model to give a detailed analysis of this phenomenon, which demonstrated that the spacing distance between the electron and hole could affect the degeneracy of  $\text{PP}^1$  and  $\text{PP}^3$  states and further affect the strength of the RISC process (i.e.,  $k_{\text{RISC}}$ ). Clearly, the spacing between the electron and hole is closely related to the concentration of guest in our DCJTB-doped OELDs. Thus, the content of DCJTB dopant would pronouncedly mediate the degenerate degree of  $\text{PP}^1$  and  $\text{PP}^3$  states and the strength of  $k_{\text{RISC}}$ , which can be reflected by our MEL detection technique. Notably, although  $k_{\text{RISC}}$  increases with reducing the dopant concentration of DCJTB, the rate constant  $k_{\text{RISC}}$  of the RISC process refers to the conversion frequency ( $\text{s}^{-1}$ ) from  $\text{PP}^3$  to  $\text{PP}^1$  in DCJTB molecules, but is not the rate ( $\text{cm}^{-3} \text{s}^{-1}$ ) of change in concentration with time.

As shown in Fig. 5(c), when the DCJTB concentration is low (2% and 5%), the electrons and holes in the DCJTB molecules are separated by one or more host molecules (red dotted frame), and the exchange splitting of PP states is negligible, resulting in degenerate  $\text{PP}^1$  and  $\text{PP}^3$  states. In this case, the RISC process of  $\text{PP}^3$  to  $\text{PP}^1$  dominates [Fig. 5(c)], as demonstrated by the low-field sharp-decrease components of the bottom two curves in Fig. 5(b). When the DCJTB concentration is increased (8%, 10%, and 16%), the electrons and holes occupy neighboring DCJTB molecules [blue dotted frame, Fig. 5(d)], and the exchange splitting of PP states is typically larger than that of the thermal energy. This leads to a larger energy gap between  $\text{PP}^1$  and  $\text{PP}^3$  states and a dominant ISC process of  $\text{PP}^1$  to  $\text{PP}^3$  [Fig. 5(d)], as proved by the low-field sharp-increase components of the top three curves in Fig. 5(b). Additionally, we obtain similar concentration-dependent MEL curves from TCTA:x% DCJTB to those of devices with the exciplex as a host (TCTA:PO-T2T:x% DCJTB) (Fig. S2 within the Supplemental Material [28]), which verifies the above conclusions.

To intuitively understand the various mechanisms occurring at different DCJTB concentrations, we fit the concentration-dependent MEL curves of Fig. 5(b) with Eq.

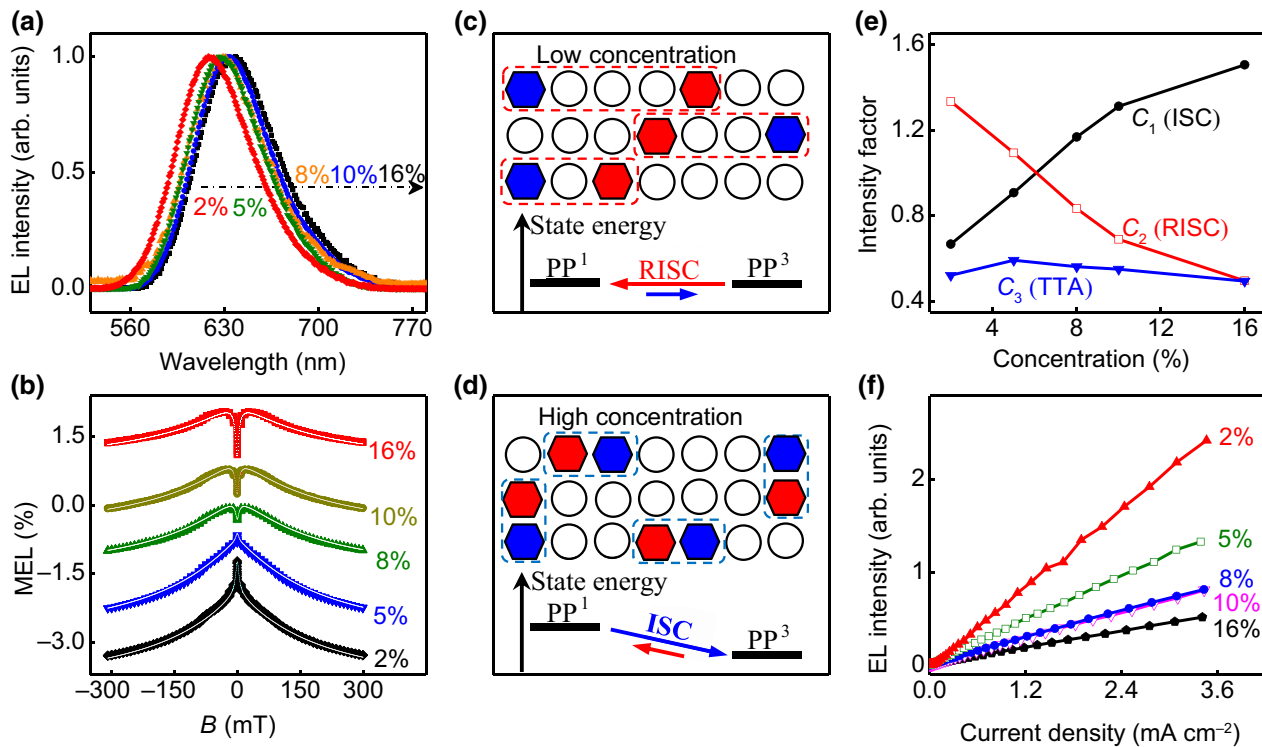


FIG. 5. (a) Normalized EL spectra of DCJTB-doped devices for different doping concentrations. (b) Concentration-dependent MEL curves of DCJTB-doped devices at 300 K and 0.833 mA/cm<sup>2</sup>. MEL curves are offset for clear observation. White solid lines are the fitted curves from DCJTB-doped devices. (c),(d) Distribution schematics of both host (circles) and guest (hexagons) molecules. Electrons (blue) and holes (red) occupy individual guest molecules, and their relative energies of singlet and triplet states vary with the distance between electron and hole. (e) Relationship between the intensity factors ( $C_1$ ,  $C_2$ , and  $C_3$ ) and the concentration of DCJTB dopant. (f) Brightness–current-density characteristics at different DCJTB concentrations.

(1) and obtain the fitting results shown in Figs. 5(b) and 5(e). It is found that ISC is enhanced and RISC is weakened with increasing DCJTB concentrations in Fig. 5(e), which are the same conclusions as obtained above. However, TTA remains insensitive to a change in DCJTB concentrations. This is because, although DET and the number of triplet excitons are enhanced with increasing DCJTB concentration, only part of the triplet excitons can be used to generate delayed fluorescence due to TTA processes, as schematically shown in Fig. S3 within the Supplemental Material [28]. Another part of triplet excitons is consumed by some other reactions with electrons or holes, i.e., the scattering channel or the dissociation channel of the TQA process [14,45], and it is reported that TQA is a dominant process over that of TTA in OLEDs [45]. Moreover, concentration quenching, as mentioned above, is also a way for triplet excitons to be consumed. Therefore, the comprehensive effects of the above three aspects determine that the strength of TTA remains almost unchanged with increasing DCJTB content in our DCJTB-doped devices.

It is expected that the variation of ISC to RISC process with decreasing DCJTB content will directly determine the enhanced EL intensity and EQE of DCJTB-doped devices, as confirmed by Fig. 5(f) and Fig. S4 within the

Supplemental Material [28]. Specifically, as shown in Fig. 5(f), the EL intensities of devices are improved by half an order of magnitude when the DCJTB concentrations are reduced from 8% to 2%. Moreover, Fig. S4 within the Supplemental Material [28] reveals that the EQE of DCJTB-doped OLEDs is enhanced by an order of magnitude (from ~1% to 10.2%) when the DCJTB content is decreased from 10% to 0.5%. Therefore, the improved EL intensity in Fig. 5(f) and the record-high EQE of 10.2% in Fig. S4 within the Supplemental Material [28] demonstrate that the EL efficiency performance of our DCJTB-based device with the dominant RISC channel of polaron pairs ( $PP_1 PP_3$ ) is indeed enhanced.

## E. MEL traces of DCJTB-doped devices with different hosts

Notably, host materials with different triplet exciton energies may affect the energy transfer of excited states between host and guest. For example, the energy back-transfer from guest to host will occur when the triplet exciton energy of guest is near to that of host, which can be reflected by our MEL results. To investigate the influence of host materials on the MEL curves in DCJTB-doped

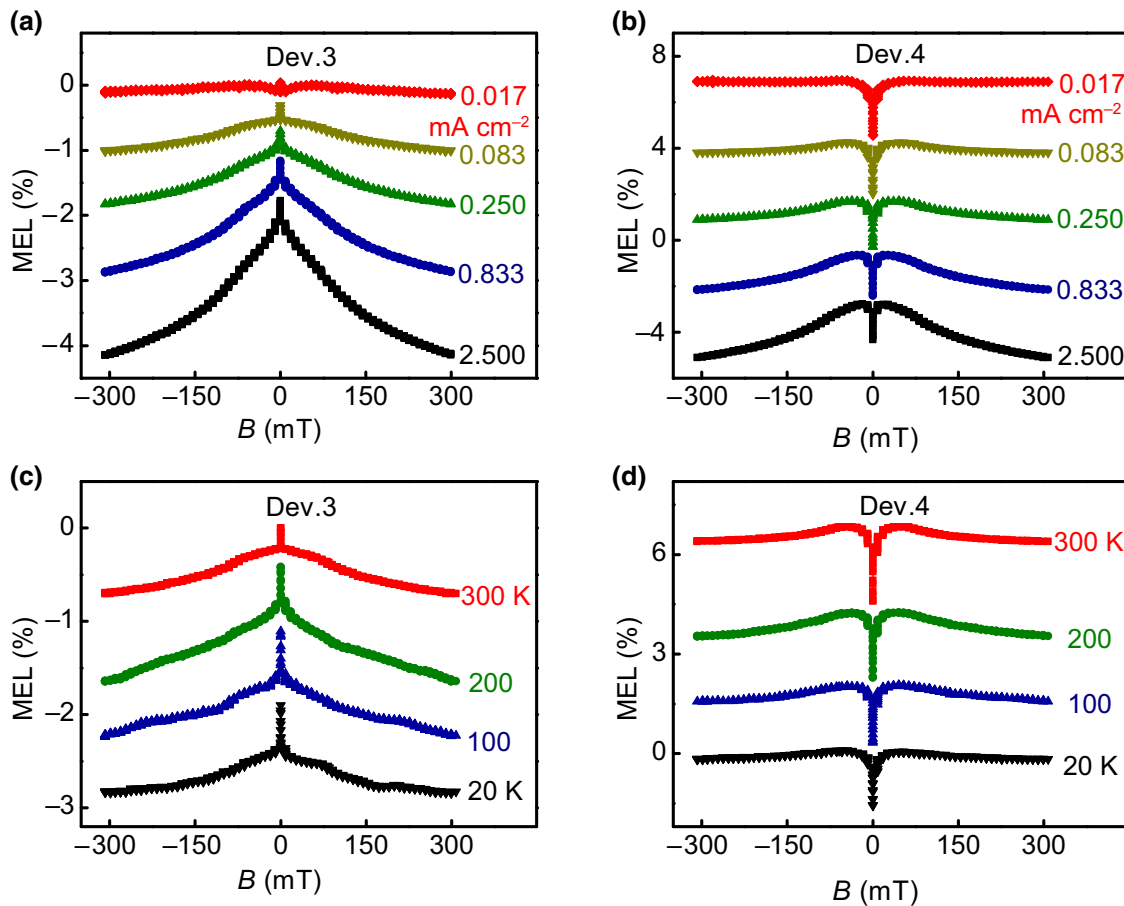


FIG. 6. Current-density- and temperature-MEL curves of Dev. 3 (a),(b) and Dev. 4 (c),(d). MEL curves are offset for clear observation.

devices, we prepare Dev. 3 and Dev. 4, with emission layers of TCTA:5%DCJTB and Alq<sub>3</sub>:5%DCJTB, respectively, while keeping other functional layers unchanged, and their current-density- and temperature-dependent MEL curves are displayed in Fig. 6. On the whole, Dev. 3 and Dev. 4 have the same line shapes of high-field MEL traces as those of Dev. 1 (TCTA:PO-T2T:5%DCJTB) for various current densities and temperatures, i.e., each MEL trace exhibits a slow decrease with increasing  $B$ . As described above, these features result from  $B$ -mediated TTA processes occurring in these three devices, due to trapping effects of the DCJTB dopant. Clearly, the most different features of MEL traces from Dev. 1 to Dev. 3 and Dev. 4 are reflected by their low-field components. It is noteworthy that Dev. 3 has the same line shapes of the low-field MEL traces as those of Dev. 1, which exhibits a rapid decrease with increasing  $B$  (i.e., features of the RISC process). This is understandable because Dev. 1 has the bulk exciplex (TCTA:PO-T2T) as the host, and Dev. 3 has TCTA:DCJTB as the emission layer and PO-T2T as the electron-transporting layer with the interface exciplex (TCTA/PO-T2T) as the host. Thus, it is not strange for

Dev. 1 and Dev. 3 to have the same line shapes of low-field MEL curves and similar current-density- and temperature-dependent MEL curves because they have similar hosts. On the contrary, the low-field MEL traces of Dev. 4, showing a rapid increase with increasing  $B$  (i.e., a feature of ISC process), are opposite to those of Dev. 1 and Dev. 3. Moreover, these low-field MEL curves of Dev. 4 display normal current density and temperature dependences, which decrease with increasing current density and drop with decreasing temperature. According to the above analyses, when the DCJTB concentration is low, the interconversions of degenerate PP<sup>1</sup> and PP<sup>3</sup> states in the DCJTB molecule are governed by the RISC process (PP<sup>3</sup>  $\rightarrow$  PP<sup>1</sup>). Therefore, the occurrence of the ISC process in Dev. 4, with Alq<sub>3</sub> as a host, needs to be interpreted in detail.

It is well known that host materials with relatively low triplet exciton energy can lead to energy loss of guest excitons in the host-guest doping system. In Dev. 4, the triplet energy of host Alq<sub>3</sub> (2.05 eV [65]) is very close to that of guest DCJTB (1.97 eV [20]), which facilitates the back-transfer of triplet excitons from guest DCJTB to

neighboring host Alq<sub>3</sub>. This may cause enhanced rate constants,  $k_T$ , of the DCJTB molecule [34,66]. When  $k_T$  is improved to be larger than that of  $k_S$ , the mainstream direction of spin mixing will change from PP<sup>3</sup> → PP<sup>1</sup> (RISC process in Dev. 3) to PP<sup>1</sup> → PP<sup>3</sup> (ISC process in Dev. 4). Clearly, host material TCTA, the triplet energy of which is very high, up to 2.85 eV [67], can effectively prevent DCJTB triplet energy transfer back to the host in Dev. 3. Therefore, it is concluded that, under a low doping concentration, host materials with different triplet exciton energies can regulate the mainstream direction of spin mixing of DCJTB polaron pairs. That is, ISC of PP<sup>1</sup> → PP<sup>3</sup> is dominant when the triplet energy difference between the host and DCJTB is small, otherwise the RISC process of PP<sup>3</sup> → PP<sup>1</sup> is governing.

#### IV. CONCLUSION

An abnormal RISC phenomenon of polaron pairs, which is enhanced with increasing current density and rises with decreasing temperature, is observed from the DCJTB-doped exciplex (TCTA:PO-T2T) based devices. More intriguingly, the transition from RISC (PP<sup>3</sup> → PP<sup>1</sup>) to ISC (PP<sup>1</sup> → PP<sup>3</sup>) is obtained through varying the electron-hole distance of polaron-pair states via increasing the DCJTB doping concentrations, which is in sharp contrast to traditional concentration-dependent RISC processes (CT<sup>3</sup> → CT<sup>1</sup>) for CT materials. In addition, ISC of exciplex polaron pairs and TTA of DCJTB excitons coexist in these DCJTB-doped devices. The interconversions of these three spin-pair states (i.e., RISC, ISC, and TTA) are closely dependent on the ET and DCT processes. Additionally, we find that host materials with different triplet exciton energies have a significant influence on the formation of spin-pair states in DCJTB-doped devices, that is, a higher triplet exciton energy of the host than that of DCJTB can ensure the efficient occurrence of RISC. This work gives valuable insights into the microscopic mechanisms of excited states of DCJTB molecules and paves the way to design high-efficiency red-light-emitting OLEDs via employing conventional fluorescent dopants with intrinsic stability.

#### ACKNOWLEDGMENTS

This work is supported by the National Foundation (NSF) of China (Grants No. 11874305 and No. 11374242), the National Science Foundation of Chongqing (Grant No. cstc2019jcyj-msxm0953), and the Science and Technology Research Program of Chongqing Municipal Education Commission (Grant No. KJQN201800510).

organic electroluminescence through Two paths of cold and Hot excitons, *Adv. Opt. Mater.* **2**, 510 (2014).

- [2] Y. J. Pu, G. Nakata, F. Satoh, H. Sasabe, D. Yokoyama, and J. Kido, Optimizing the charge balance of fluorescent organic light-emitting devices to achieve high external quantum efficiency beyond the conventional upper limit, *Adv. Mater.* **24**, 1765 (2012).
- [3] Y. S. Park, S. Lee, K. H. Kim, S. Y. Kim, J. H. Lee, and J. J. Kim, Exciplex-Forming Co-host for organic light-emitting diodes with ultimate efficiency, *Adv. Funct. Mater.* **23**, 4914 (2013).
- [4] S. Lee, K. H. Kim, D. Limbach, Y. S. Park, and J. J. Kim, Low roll-Off and high efficiency orange organic light emitting diodes with controlled Co-doping of green and Red phosphorescent dopants in an exciplex forming Co-host, *Adv. Funct. Mater.* **23**, 4105 (2013).
- [5] H. Shin, S. Lee, K. H. Kim, C. K. Moon, S. J. Yoo, J. H. Lee, and J. J. Kim, Blue phosphorescent organic light-emitting diodes using an exciplex forming Co-host with the external quantum efficiency of theoretical limit, *Adv. Mater.* **26**, 4730 (2014).
- [6] J. W. Sun, J. H. Lee, C. K. Moon, K. H. Kim, H. Shin, and J. J. Kim, A fluorescent organic light-emitting diode with 30% external quantum efficiency, *Adv. Mater.* **26**, 5684 (2014).
- [7] H. Uoyama, K. Goushi, K. Shizu, H. Nomura, and C. Adachi, Highly efficient organic light-emitting diodes from delayed fluorescence, *Nature* **492**, 234 (2012).
- [8] K. Goushi, K. Yoshida, K. Sato, and C. Adachi, Organic light-emitting diodes employing efficient reverse intersystem crossing for triplet-to-singlet state conversion, *Nat. Photonics* **6**, 253 (2012).
- [9] K. Goushi and C. Adachi, Efficient organic light-emitting diodes through up-conversion from triplet to singlet excited states of exciplexes, *Appl. Phys. Lett.* **101**, 023306 (2012).
- [10] B. Zhao, T. Y. Zhang, B. Chu, W. L. Li, Z. S. Su, H. R. Wu, X. W. Yan, F. M. Jin, Y. Gao, and C. Y. Liu, Highly efficient red OLEDs using DCJTB as the dopant and delayed fluorescent exciplex as the host, *Sci. Rep.* **5**, 10697 (2015).
- [11] N. L. Zhou, S. R. Wang, Y. Xiao, and X. G. Li, Double light-emitting layer implementing three-color emission: Using DCJTB lightly doping in Alq<sub>3</sub> as red-green emitting layer and APEAn1N as blue-green emitting layer, *J. Lumin.* **196**, 40 (2018).
- [12] W. P. Gillin, S. J. Zhang, N. J. Rolfe, P. Desai, P. Shakya, A. J. Drew, and T. Kreouzis, Determining the influence of excited states on current transport in organic light emitting diodes using magnetic field perturbation, *Phys. Rev. B* **82**, 195208 (2010).
- [13] T. T. Zhang, D. F. Holford, H. Gu, T. Kreouzis, S. J. Zhang, and W. P. Gillin, Hole-exciton interaction induced high field decay of magneto-electroluminescence in Alq(3)-based organic light-emitting diodes at room temperature, *Appl. Phys. Lett.* **108**, 023303 (2016).
- [14] X. T. Tang, Y. Q. Hu, W. Y. Jia, R. H. Pan, J. Q. Deng, Z. H. He, and Z. H. Xiong, Intersystem crossing and triplet fusion in singlet-fission-dominated rubrene-based OLEDs under high bias current, *ACS Appl. Mater. Interfaces* **10**, 1948 (2018).
- [15] S. A. Crooker, F. Liu, M. R. Kelley, N. J. D. Martinez, W. Nie, A. Mohite, I. H. Nayyar, S. Tretiak, D. L. Smith,

[1] Y. Y. Pan, W. J. Li, S. T. Zhang, L. Yao, C. Gu, H. Xu, B. Yang, and Y. G. Ma, High yields of singlet excitons in

- and P. P. Ruden, Spectrally resolved hyperfine interactions between polaron and nuclear spins in organic light emitting diodes: Magneto-electro-luminescence studies, *Appl. Phys. Lett.* **105**, 153304 (2014).
- [16] Q. S. Zhang, J. Li, K. Shizu, S. P. Huang, S. Hirata, H. Miyazaki, and C. Adachi, Design of efficient thermally activated delayed fluorescence materials for pure blue organic light emitting diodes, *J. Am. Chem. Soc.* **134**, 14706 (2012).
- [17] L. Zhang and K. W. Cheah, Thermally activated delayed fluorescence host for high performance organic light-emitting diodes, *Sci. Rep.* **8**, 8832 (2018).
- [18] P. Chen, L. P. Wang, W. Y. Tan, Q. M. Peng, S. T. Zhang, X. H. Zhu, and F. Li, Delayed fluorescence in a solution-processable pure Red molecular organic emitter based on dithienylbenzothiadiazole: A joint optical, electroluminescence, and magnetoelectroluminescence study, *ACS Appl. Mater. Interfaces* **7**, 2972 (2015).
- [19] Y. Luo and H. Aziz, Correlation between triplet triplet annihilation and electroluminescence efficiency in doped fluorescent organic light-emitting devices, *Adv. Funct. Mater.* **20**, 1285 (2010).
- [20] P. Chen, Z. H. Xiong, Q. M. Ping, J. W. Bai, S. T. Zhang, and F. Li, Magneto-Electroluminescence as a tool to discern the origin of delayed fluorescence: Reverse intersystem crossing or triplet-triplet annihilation?, *Adv. Opt. Mater.* **2**, 142 (2014).
- [21] H. Nakanotani, T. Furukawa, K. Morimoto, and C. Adachi, Long-range coupling of electron-hole pairs in spatially separated organic donor-acceptor layers, *Sci. Adv.* **2**, 2 (2016).
- [22] J. H. Lee, S. H. Cheng, S. J. Yoo, H. Shin, J. H. Chang, C. I. Wu, K. T. Wong, and J. J. Kim, An exciplex forming host for highly efficient blue organic light emitting diodes with Low driving voltage, *Adv. Funct. Mater.* **25**, 361 (2015).
- [23] Y. F. Zhang and S. R. Forrest, Triplet diffusion leads to triplet-triplet annihilation in organic phosphorescent emitters, *Chem. Phys. Lett.* **590**, 106 (2013).
- [24] H. van Eersel, P. A. Bobbert, and R. Coehoorn, Kinetic Monte Carlo study of triplet-triplet annihilation in organic phosphorescent emitters, *J. Appl. Phys.* **117**, 115502 (2015).
- [25] Y. Kawamura, J. Brooks, J. J. Brown, H. Sasabe, and C. Adachi, Intermolecular Interaction and a Concentration-Quenching Mechanism of Phosphorescent Ir(III) Complexes in a Solid Film, *Phys. Rev. Lett.* **96**, 017404 (2006).
- [26] H. Oevering, J. W. Verhoeven, M. N. Paddonrow, E. Cottaris, and N. S. Hush, Long-Range exchange contribution to singlet-singlet energy transfer in a series of rigid bichromophoric molecules, *Chem. Phys. Lett.* **143**, 488 (1988).
- [27] A. Kirch, M. Gmelch, and S. Reineke, Simultaneous singlet-singlet and triplet-singlet Förster resonance energy transfer from a single donor material, *J. Phys. Chem. Lett.* **10**, 310 (2019).
- [28] See the Supplemental Material at <http://link.aps.org/supplemental/10.1103/PhysRevApplied.14.024011> for additional data descriptions of various interactions between the triplet exciton and charges or polarons, and the formation mechanisms of MEL traces induced from *B*-mediated interconversions of spin-pair states.
- [29] L. X. Chen, W. Y. Jia, Y. B. Chen, J. Xiang, D. Y. Liu, and Z. H. Xiong, Simultaneous sign change of magneto-electroluminescence and magneto-conductance in polymer/colloidal quantum Dot nanocomposites, *J. Phys. Chem. C* **121**, 8128 (2017).
- [30] Y. Iwasaki, T. Osasa, M. Asahi, M. Matsumura, Y. Sakaguchi, and T. Suzuki, Fractions of singlet and triplet excitons generated in organic light-emitting devices based on a polyphenylenevinylene derivative, *Phys. Rev. B* **74**, 195209 (2006).
- [31] Q. M. Peng, A. W. Li, Y. X. Fan, P. Chen, and F. Li, Studying the influence of triplet deactivation on the singlet-triplet inter-conversion in intra-molecular charge-transfer fluorescence-based OLEDs by magneto-electroluminescence, *J. Mater. Chem. C* **2**, 6264 (2014).
- [32] G. B. Piland, J. J. Burdett, D. Kurunthu, and C. J. Bardeen, Magnetic field effects on singlet fission and fluorescence decay dynamics in amorphous rubrene, *J. Phys. Chem. C* **117**, 1224 (2013).
- [33] P. Avakian and R. E. Merrifield, Triplet excitons in anthracene crystals-A review, *Mol. Cryst. L* **5**, 37 (1968).
- [34] Y. L. Lei, Q. M. Zhang, R. Liu, P. Chen, Q. L. Song, and Z. H. Xiong, Driving current and temperature dependent magnetic-field modulated electroluminescence in Alq<sub>3</sub>-based organic light emitting diode, *Org. Electron.* **10**, 889 (2009).
- [35] Y. Zhang, R. Liu, Y. L. Lei, and Z. H. Xiong, Low temperature magnetic field effects in Alq<sub>3</sub>-based organic light emitting diodes, *Appl. Phys. Lett.* **94**, 08337 (2009).
- [36] J. Q. Deng, W. Y. Jia, Y. B. Chen, D. Y. Liu, Y. Q. Hu, and Z. H. Xiong, Guest concentration, bias current, and temperature-dependent sign inversion of magnetoelectroluminescence in thermally activated delayed fluorescence devices, *Sci. Rep.* **7**, 44396 (2017).
- [37] Q. M. Peng, W. J. Li, S. T. Zhang, P. Chen, F. Li, and Y. G. Ma, Evidence of the reverse intersystem crossing in intra-molecular charge-transfer fluorescence-based organic light-emitting devices through magneto-electroluminescence measurements, *Adv. Opt. Mater.* **1**, 362 (2013).
- [38] C. X. Zhao, W. Y. Jia, K. X. Huang, Q. M. Zhang, X. H. Yang, and Z. H. Xiong, Anomalous temperature dependent magneto-conductance in organic light-emitting diodes with multiple emissive states, *Appl. Phys. Lett.* **107**, 023302 (2015).
- [39] P. Chen, Q. M. Peng, L. Yao, and F. Li, Identifying the efficient inter-conversion between singlet and triplet charge-transfer states by magneto-electroluminescence study, *Appl. Phys. Lett.* **102**, 063301 (2013).
- [40] P. S. Yuan, X. F. Qiao, D. H. Yan, and D. G. Ma, Magnetic field effects on the quenching of triplet excitons in exciplex-based organic light emitting diodes, *J. Mater. Chem. C* **6**, 5721 (2018).
- [41] Z. W. Yu, J. X. Zhang, S. H. Liu, L. T. Zhang, Y. Zhao, H. Y. Zhao, and W. F. Xie, High-Efficiency blue phosphorescent organic light-emitting devices with Low efficiency roll-Off at ultrahigh luminance by the reduction of triplet-polaron quenching, *ACS Appl. Mater. Interfaces* **11**, 6292 (2019).
- [42] H. van Eersel, P. A. Bobbert, R. A. J. Janssen, and R. Coehoorn, Effect of Förster-mediated triplet-polaron

- quenching and triplet-triplet annihilation on the efficiency roll-Off of organic light-emitting diodes, *J. Appl. Phys.* **119**, 163102 (2016).
- [43] W. Y. Jia, Q. S. Chen, Y. B. Chen, L. X. Chen, and Z. H. Xiong, Magneto-Conductance characteristics of trapped triplet-polaron and triplet-trapped polaron interactions in anthracene-based organic light emitting diodes, *Phys. Chem. Chem. Phys.* **18**, 30733 (2016).
- [44] A. Obolda, Q. M. Peng, C. Y. He, T. Zhang, J. J. Ren, H. W. Ma, Z. G. Shuai, and F. Li, Triplet-polaron-interaction-induced upconversion from triplet to singlet: A possible Way to obtain highly efficient OLEDs, *Adv. Mater.* **28**, 4740 (2016).
- [45] M. Shao, L. Yan, M. X. Li, I. Ilia, and B. Hu, Triplet-charge annihilation versus triplet-triplet annihilation in organic semiconductors, *J. Mater. Chem. C* **1**, 1330 (2013).
- [46] Y. B. Chen, W. Y. Jia, J. Xiang, D. Yuan, Q. S. Chen, L. X. Chen, and Z. H. Xiong, Identify triplet-charge interaction in rubrene-based diodes using magneto-conductance: Coexistence of dissociation and scattering channels, *Org. Electron.* **39**, 207 (2016).
- [47] J. Appel, Polarons, *Solid State Phys.* **21**, 193 (1968).
- [48] P. Calvani, Optical properties of polarins, *Riv. del Nuovo Cim. Della Soc. Italiana Fisica* **24**, 1 (2001).
- [49] K. Buse, J. Imbrock, E. Kratzig, and K. Peithmann, *Photorefractive Effects in LiNbO<sub>3</sub> and LiTaO<sub>3</sub>* (Springer, Berlin, 2007), pp. 83.
- [50] J. T. Devreese, Polarons, *Ency. Appl. Phys.* **14**, 383 (1994).
- [51] T. D. Nguyen, T. P. Basel, Y. J. Pu, X. G. Li, E. Ehrenfreund, and Z. V. Vardeny, Isotope effect in the spin response of aluminum tris(8-hydroxyquinoline) based devices, *Phys. Rev. B: Condens. Matter. Mater. Phys.* **85**, 245437 (2012).
- [52] T. D. Nguyen, G. Hukic-Markosian, F. Wang, L. Wojcik, X. G. Li, E. Ehrenfreund, and Z. V. Vardeny, Isotope effect in spin response of pi-conjugated polymer films and devices, *Nat. Mater.* **9**, 345 (2010).
- [53] W. Y. Jia, Q. S. Chen, L. X. Chen, D. Yuan, J. Xiang, Y. B. Chen, and Z. H. Xiong, Molecular spacing modulated conversion of singlet fission to triplet fusion in rubrene-based organic light-emitting diodes at ambient temperature, *J. Phys. Chem. C* **120**, 8380 (2016).
- [54] K. W. Tsai, T. H. Lee, J. H. Wu, J. Y. Jhou, W. S. Huang, S. N. Hsieh, T. C. Wen, T. F. Guo, and J. C. A. Huang, Antagonistic responses between magnetoconductance and magnetoelectroluminescence in polymer light-emitting diodes, *Org. Electron.* **14**, 1376 (2013).
- [55] R. H. Pan, X. T. Tang, Y. Q. Hu, H. Q. Zhu, J. Q. Deng, and Z. H. Xiong, Extraordinary magnetic field effects mediated by spin-pair interaction and electron mobility in thermally activated delayed fluorescence-based OLEDs with quantum-well structure, *J. Mater. Chem. C* **7**, 2421 (2019).
- [56] S. P. Kersten, A. J. Schellekens, B. Koopmans, and P. A. Bobbert, Magnetic-Field Dependence of the Electroluminescence of Organic Light-Emitting Diodes: A Competition Between Exciton Formation and Spin Mixing, *Phys. Rev. Lett.* **106**, 197402 (2011).
- [57] J. Xiang, Y. B. Chen, W. Y. Jia, L. X. Chen, Y. L. Lei, Q. M. Zhang, and Z. H. Xiong, Realization of triplet-triplet annihilation in planar heterojunction exciplex-based organic light-emitting diodes, *Org. Electron.* **28**, 94 (2016).
- [58] S. Baniya, Z. Y. Pang, D. Sun, Y. X. Zhai, O. Kwon, H. Choi, B. Choi, S. Lee, and V. Vardeny, Magnetic field effect in organic light-emitting diodes based on electron donor-acceptor exciplex chromophores doped with fluorescent emitters, *Adv. Funct. Mater.* **26**, 6930 (2016).
- [59] Y. C. Hsiao, T. Wu, M. X. Li, and B. Hu, Magneto-Optical studies on spin-dependent charge recombination and dissociation in perovskite solar cells, *Adv. Mater.* **27**, 2899 (2015).
- [60] G. Y. Zhong, Z. Xu, J. He, S. T. Zhang, Y. Q. Zhan, X. J. Wang, Z. H. Xiong, H. Z. Shi, and X. M. Ding, Aggregation and permeation of 4-(dicyanomethylene)-2-methyl-6-(p-dimethylaminostyryl)-4H-pyran molecules in Alq<sub>3</sub>, *Appl. Phys. Lett.* **81**, 1122 (2002).
- [61] S. W. Feng, M. C. Shih, C. J. Huang, and C. T. Chung, Impacts of dopant concentration on the carrier transport and recombination dynamics in organic light emitting diodes, *Thin Solid Films* **27**, 2719 (2009).
- [62] E. Hontz, W. D. Chang, D. N. Congreve, V. Bulović, M. A. Baldo, and T. V. Voorhis, The role of electron-hole separation in thermally activated delayed fluorescence in donor-acceptor blends, *J. Phys. Chem. C* **119**, 25591 (2015).
- [63] P. B. Deotare, W. Chang, E. Hontz, D. N. Congreve, L. Shi, P. D. Reusswig, B. Modtland, M. E. Bahlke, C. K. Lee, A. P. Willard, V. Bulović, T. Van Voorhis, and M. A. Baldo, Nanoscale transport of charge-transfer states in organic donor-acceptor blends, *Nat. Mater.* **14**, 1130 (2015).
- [64] C. K. Lee, L. Shi, and A. P. Willard, A model of charge-transfer excitons: Diffusion, spin dynamics, and magnetic field effects, *J. Phys. Chem. Lett.* **7**, 2246 (2016).
- [65] J. Kalinowski, M. Cocchi, D. Virgili, P. D. Marco, and V. Fattori, Magnetic field effects on emission and current in Alq(3)-based electroluminescent diodes, *Chem. Phys. Lett.* **380**, 710 (2003).
- [66] Y. Wu, Z. H. Xu, and B. Hu, Tuning magnetoresistance and magnetic-field-dependent electroluminescence through mixing a strong-spin-orbital-coupling molecule and a weak-spin-orbital-coupling polymer, *Phys. Rev. B* **75**, 035214 (2007).
- [67] T. T. Lu, W. Jiang, K. Y. Sun, W. W. Tian, and Y. M. Sun, Reduced efficiency roll-off and enhanced excitation confinement in exciplex-type host: Electron transport materials based on benzimidazole units, *Dyes Pigm.* **151**, 35 (2018).